APL Materials

RESEARCH ARTICLE | JULY 12 2024

Magnetic and magneto-transport properties of non-collinear antiferromagnetic Mn_3Ge epitaxial films

Yutaro Takeuchi ; Hossein Sepehri-Amin ; Satoshi Sugimoto ; Takanobu Hiroto ; Shinya Kasai

Check for updates

APL Mater. 12, 071110 (2024)
https://doi.org/10.1063/5.0217710

View Online
Export Citation

15 July 2024 07:27:53

AMERICAN ELEMENTS
THE MATERIALS SCIENCE MANUFACTURER®
Now Invent.™
27 ANNIVERSARY
American Elements
Opens a World of Possibilities
...Now Invent!
www.americanelements.com

AIP Publishing

Magnetic and magneto-transport properties of non-collinear antiferromagnetic Mn_3Ge epitaxial films

Cite as: APL Mater. 12, 071110 (2024); doi: 10.1063/5.0217710
Submitted: 6 May 2024 • Accepted: 1 July 2024 •
Published Online: 12 July 2024

View Online Export Citation CrossMark

Yutaro Takeuchi,[1,a)] Hossein Sepehri-Amin,[2] Satoshi Sugimoto,[2] Takanobu Hiroto,[3] and Shinya Kasai[2,a)]

AFFILIATIONS

[1] International Center for Young Scientists (ICYS), National Institute for Materials Science (NIMS), Tsukuba 305-0047, Japan
[2] Research Center for Magnetic and Spintronic Materials, National Institute for Materials Science (NIMS), Tsukuba 305-0047, Japan
[3] Research Network and Facility Services Division, National Institute for Materials Science, Tsukuba 305-0047, Japan

[a)] **Authors to whom correspondence should be addressed:** takeuchi.yutaro@nims.go.jp and kasai.shinya@nims.go.jp

ABSTRACT

Antiferromagnetic Mn_3X (X = Sn, Ge, Ga, and Pt) possessing non-collinear spin structures with Kagome lattices have attracted increasing interest because of their unique properties, such as significant anomalous Hall and magneto-optical Kerr effects. Recent advances in spintronic devices that use non-collinear antiferromagnets have inspired research into various materials for exploiting their potential. In this study, we investigated the magnetic and magneto-transport properties of $(1\bar{1}00)$-oriented epitaxial and polycrystalline Mn_3Ge films deposited by magnetron sputtering. Anomalous Hall conductivity monotonically decreases with temperature in an epitaxial Mn_3Ge film, whereas the polycrystalline sample demonstrates a different trend. Furthermore, we obtained a large in-Kagome-plane uniaxial magnetic anisotropy of epitaxial Mn_3Ge above ambient temperature, thereby leading to higher thermal stability and robustness against the external field. Our results indicate the potential of Mn_3Ge for future functional, high-speed, and high-density spintronics devices using antiferromagnets.

© 2024 Author(s). All article content, except where otherwise noted, is licensed under a Creative Commons Attribution (CC BY) license (https://creativecommons.org/licenses/by/4.0/). https://doi.org/10.1063/5.0217710

15 July 2024 07:27:53

The progress in spintronics research demonstrated notable potential in nonvolatile memories and unconventional computing technology.[1–3] Ferromagnets are commonly used as components of such functional devices, thereby resulting in spintronic effects. In addition, antiferromagnets have recently attracted growing interest because of their unique attributes, such as negligible stray fields, robustness to external magnetic fields, and high-speed spin dynamics. These characteristics created a new paradigm in spintronics called antiferromagnetic spintronics.[4–7] In particular, antiferromagnetic orderings with macroscopically broken time-reversal symmetry cause intriguing topological phenomena.[8–11] Mn_3X (X = Sn, Ge, Ga, and Pt) antiferromagnets have a non-collinear magnetic texture in the Kagome lattice and exhibit the large anomalous Hall effect (AHE)[8,9] and magneto-optical Kerr effect[12] arising from the Berry curvature in momentum spaces. Among these antiferromagnets, hexagonal $D0_{19}$-Mn_3Ge shows significant anomalous Hall conductivity,[9,13] and recent studies have reported long-range supercurrents in Josephson junctions at the Mn_3Ge/Nb interface.[14,15]

Topologically nontrivial effects of non-collinear antiferromagnets have been observed not only in bulk single crystals but also in thin films in recent years.[16–24] Such studies led to the current-induced control of magnetic texture[25–31] in hexagonal Mn_3Sn and the observation of the magnetoresistance effect of antiferromagnetic tunnel junctions with Mn_3Sn[32] and cubic Mn_3Pt.[33] Epitaxial films with the Kagome plane oriented normal to the film plane are desired to further investigate the functionalities of non-collinear antiferromagnets. These material systems can offer various favorable conditions, for example, an optimal configuration for spin-orbit torque (SOT)-induced switching,[29,31] rotation of magnetic texture,[26]

© Author(s) 2024

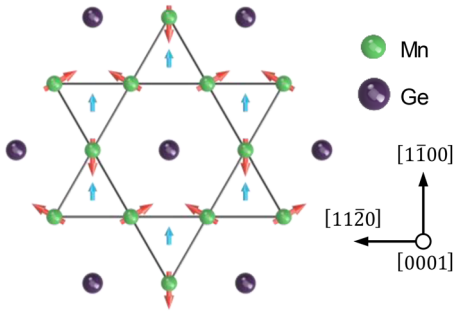

FIG. 1. Crystal structure and magnetic texture of Mn atoms in the (0001) plane (Kagome plane) of $D0_{19}$-Mn_3Ge. The red and light blue arrows denote local magnetic moments of Mn atoms and the magnetic order parameter, respectively.

and evaluation of magnetic anisotropies[31] in non-collinear antiferromagnets. However, the epitaxial growth of non-collinear antiferromagnets is technically challenging, and only a few stacks with the $(1\bar{1}00)$ plane [M-plane]-oriented $D0_{19}$-Mn_3Sn[22,26] and Mn_3Ga[24] films have been demonstrated. Despite the outstanding potential of Mn_3Ge, studies on the properties of its thin films have been limited to polycrystalline[34–36] and C-plane-oriented[37,38] films. The challenging aspect of Mn_3Ge deposition is the presence of hexagonal $D0_{19}$ and tetragonal $D0_{22}$ phases with different magnetic structures, which are stable at high and low temperatures, respectively.[36] Therefore, performing the deposition using underlayers with a small lattice mismatch at appropriate temperatures is necessary to obtain single-phase non-collinear antiferromagnetic $D0_{19}$-Mn_3Ge films. Here, we developed a sputter deposition technique for $(1\bar{1}00)$ plane-oriented non-collinear antiferromagnetic Mn_3Ge epitaxial films on a MgO(110) substrate/W and investigated their magnetic and magneto-transport properties. The (0001) plane of the family of hexagonal $D0_{19}$-Mn_3Ge, Mn_3Sn, and Mn_3Ga constitutes a Kagome lattice of Mn atoms, whose magnetic moment forms an antiferromagnetic chiral spin structure attributed to geometrical frustration and the Dzyaloshinskii–Moriya interaction (Fig. 1). In this structure, the local uniaxial anisotropy induces a small uncompensated magnetic moment and global sixfold magnetic anisotropy.[39–41] The Dzyaloshinskii–Moriya interaction determines the chirality of non-collinear spin texture and contributes to the out-of-Kagome-plane magnetic anisotropy.[41] Furthermore, recent studies have shown global two- and fourfold magnetic anisotropies originating from tensile strain in the Kagome plane.[29,31] In this study, we investigated the temperature dependence of the AHE and magnetic anisotropies in epitaxial Mn_3Ge films. The obtained properties are discussed, along with the results for polycrystalline Mn_3Ge films deposited on the MgO(100) substrate.

Stacks consisting of Mn_3Ge(50 nm)/Ta(2 nm) and W(t_W)/Mn_3Ge(50 nm)/Ta(2 nm) from the substrate side were deposited on MgO(100) and MgO(110) single-crystal substrates, respectively, using DC magnetron sputtering, where t_W denotes the thickness of the W layer [Figs. 2(a) and 2(b)]. Furthermore, W is the buffer layer for the epitaxial growth of the Mn_3Ge film and Ta is the capping layer. The deposition of Mn_3Ge is deposited by co-sputtering Mn and Ge targets. The nominal substrate temperatures of W, Mn_3Ge, and Ta layers are 400, 650, and 100 °C, respectively. The Mn content of the Mn_3Ge layer was determined to be 76.9% using inductively coupled plasma optical emission spectrometry. The crystal structures were characterized using x-ray diffraction (XRD) and scanning transmission electron microscopy (STEM). For the magneto-transport measurements, the films were processed into 40-μm-wide Hall bar devices using photolithography and Ar-ion milling. All electrical measurements were performed using a physical property measurement system.

First, we studied the crystalline structures of Mn_3Ge films with different underlayers using XRD measurements. Figure 2(c) illustrates the out-of-plane XRD patterns of a stack of MgO(100) sub./Mn_3Ge(50 nm)/Ta(2 nm). We confirmed the single-phase and three-dimensional polycrystalline nature of hexagonal $D0_{19}$-Mn_3Ge, which was also reported in a previous study.[35] Figure 2(d) illustrates the XRD patterns of MgO(110) sub./W(t_W)/Mn_3Ge(50 nm)/Ta(2 nm) for various W thicknesses. When $t_W \geq 5$ nm, we confirm peaks from $(1\bar{1}00)$, $(2\bar{2}00)$, $(3\bar{3}00)$, and $(4\bar{4}00)$ of $D0_{19}$-Mn_3Ge together with a peak from α-W(211), thereby indicating the M-plane ordering of hexagonal Mn_3Ge to

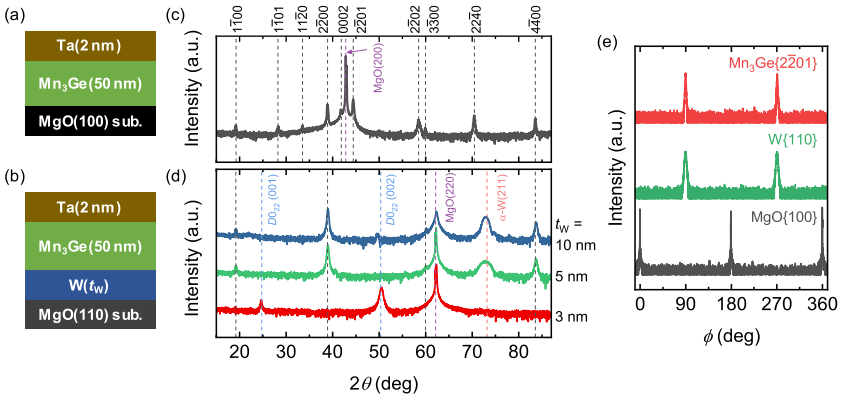

FIG. 2. Stack structures expected for (a) polycrystalline and (b) M-plane oriented Mn_3Ge films. (c) and (d) Out-of-plane XRD patterns of MgO(100) sub./Mn_3Ge(50 nm)/Ta(2) and MgO(110) sub./W(t_W)/Mn_3Ge(50 nm)/Ta(2), respectively. (e) ϕ-scan patterns of MgO substrate, W, and Mn_3Ge layers for t_W = 10 nm.

15 July 2024 07:27:53

© Author(s) 2024

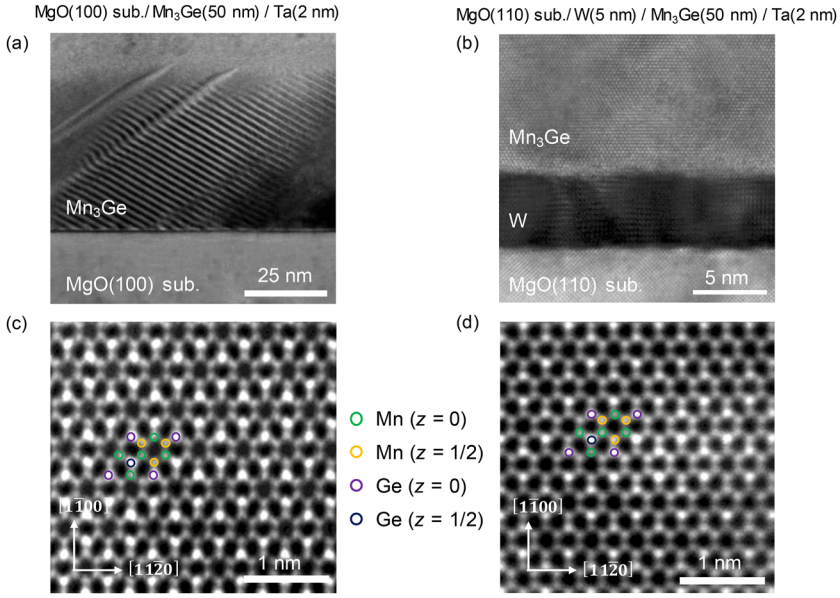

FIG. 3. Cross-sectional bright field (BF)-STEM images of stacks of (a) MgO(100) sub./Mn_3Ge(50 nm)/Ta(2 nm) and (b) MgO(110) sub./W(5 nm)/Mn_3Ge(50 nm)/Ta(2 nm). (c) and (d) Magnified high angle annular dark field (HAADF)-STEM images of the Kagome lattice in selected areas of Figs. 3(a) and 3(b), respectively. Atomic configuration is highlighted by circular symbols.

be similar to the previous studies of $D0_{19}$-Mn_3Sn on the W(211) buffer layer.[22,26] Meanwhile, when t_W = 3 nm, peaks from (001) and (002) of tetragonal $D0_{22}$-Mn_3Ge are observed together with the disappearance of the α-W(211) peak, suggesting that the amorphous W does not stabilize the growth of the $D0_{19}$ phase; however, the formation of the $D0_{22}$ structure occurs. Figure 2(e) illustrates the ϕ-scan patterns of the sample with t_W = 10 nm, where a peak is observed every 180°, as expected for the epitaxial film of the M-plane Mn_3Ge. An epitaxial relationship was identified as $MgO(110)[001]\|W(211)[01\bar{1}]\|Mn_3Ge(1\bar{1}00)[0001]$. Figure 3(a) illustrates the cross-sectional bright field (BF)-STEM image of MgO(100) sub./Mn_3Ge(50 nm)/Ta(2 nm) and MgO(110) stacks. Furthermore, we observed crystal twinning in the grains of the polycrystalline Mn_3Ge, which is consistent with the XRD measurements. Figure 3(b) illustrates the cross-sectional BF-STEM image of a MgO(110) sub./W(5 nm)/Mn_3Ge(50 nm)/Ta(2 nm) stack, where electron beams were transmitted along the direction of MgO[001], thereby indicating the layer-by-layer growth of W and Mn_3Ge layers with smooth film surfaces. High resolution high angle annular dark field (HAADF)-STEM images of the polycrystalline and epitaxial Mn_3Ge layers are presented in Figs. 3(c) and 3(d), respectively. We confirmed the clearly visible Kagome lattices and atomic configuration of hexagonal $D0_{19}$-Mn_3Ge.

Figures 4(a) and 4(b) illustrate the Hall resistance R_H as a function of the out-of-plane magnetic field H_z for the MgO(100) sub./Mn_3Ge(50 nm)/Ta(2 nm) and MgO(110) sub./W(5 nm)/Mn_3Ge(50 nm)/Ta(2 nm) stacks at a temperature T of 10–350 K. The former and latter stacks correspond to samples with polycrystalline and M-plane oriented epitaxial Mn_3Ge, respectively. A DC current of 2 mA was applied to the channel of the Hall bar devices. Here, the current density into the W layer for epitaxial samples was estimated to be less than 0.3 MA/cm^2 at 10–400 K, indicating the negligible role of current-induced spin-orbit torque.[26,29,31] The negative and zero-field anomalous Hall resistances were obtained at 10 K, except for that of the polycrystalline sample. The negative anomalous Hall resistance is consistent with the results of previous studies on the $D0_{19}$ structured non-collinear antiferromagnets. Moreover, we confirmed that the spontaneous magnetization of our Mn_3Ge film is less than ~12 mT, which is comparable to that of bulk $D0_{19}$-Mn_3Ge (Fig. S1 of the supplementary material).[9,13] Therefore, the topological spin configuration of the antiferromagnetic Mn_3Ge is responsible for the obtained AHEs.

We first evaluated the layer resistivities ρ_{xx} of the prepared stacks through channel resistance measurements in Hall bar devices to quantitatively investigate the obtained magneto-transport properties. Assuming a parallel resistance model, ρ_{xx} for the W and Mn_3Ge layers of the epitaxial films was obtained from the channel resistance vs the Mn_3Ge thickness [not shown]. The conduction of the Ta capping layer was neglected because of its insulating effect through natural oxidation. Figure 4(c) illustrates the T dependencies of ρ_{xx} for polycrystalline and epitaxial Mn_3Ge and W films. The obtained ρ_{xx} of both polycrystalline and epitaxial Mn_3Ge increased from 10 to 200 K and showed no significant change above 200 K, which is a similar trend to that of bulk Mn_3Ge.[9,13] In the polycrystalline sample, ρ_{xx} reached ~300 μΩ cm from 200 to 400 K, whereas that of the epitaxial one was below 200 μΩ cm. Accounting for the shunt current in the W buffer layer, we evaluated the zero-field transverse resistivity ρ_{xy} and anomalous Hall conductivity σ_{xy} ($= -\rho_{xy}/\rho_{xx}^2$) of the Mn_3Ge films as displayed in Figs. 4(d)

15 July 2024 07:27:53

© Author(s) 2024

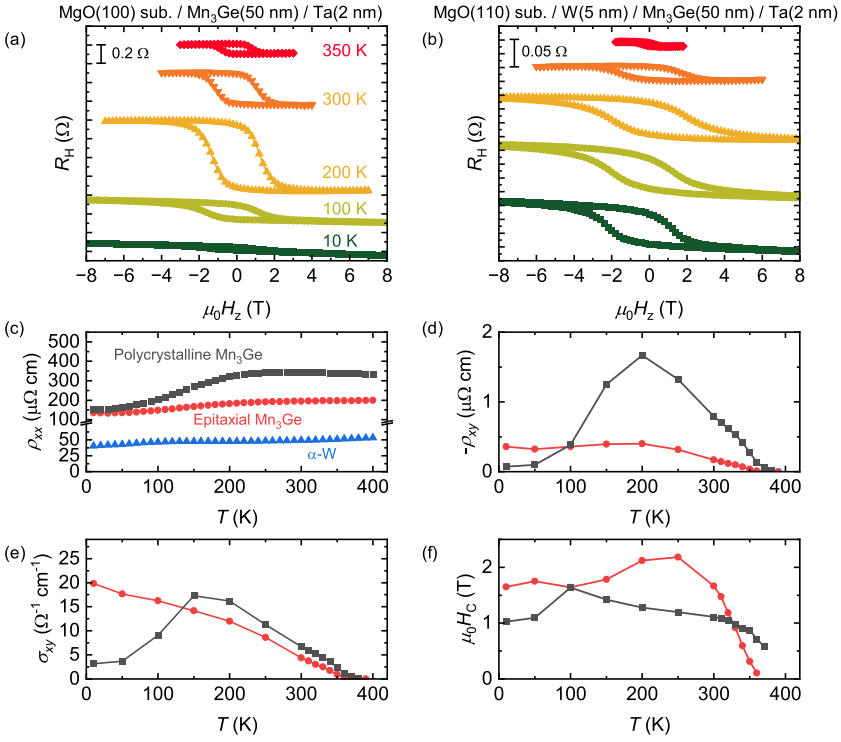

FIG. 4. Hall resistance R_H as a function of out-of-plane magnetic field H_z in Hall bar devices with (a) MgO(100) sub./Mn_3Ge(50 nm)/Ta(2 nm) and (b) MgO(110) sub./W(5 nm)/Mn_3Ge(50 nm)/Ta(2 nm) at different T, where μ_0 represents the permeability in a vacuum. T dependence of (c) ρ_{xx}, (d) ρ_{xy}, (e) σ_{xy}, and (d) $\mu_0 H_C$ for each layer of stacks. The black square, red circular, and blue triangular symbols denote those for polycrystalline Mn_3Ge, epitaxial Mn_3Ge, and α-W layers, respectively.

and 4(e), respectively. σ_{xy} is insensitive to ρ_{xx} in the system, suggesting the main role of the intrinsic AHE originating from the Berry curvature in the momentum spaces. The AHE of both samples vanishes at $T \sim 380$ K, which is consistent with the Néel temperature of bulk Mn_3Ge.[9,13] At temperatures above 200 K, the magnitude of σ_{xy} shows a small difference between two samples, whereas the ρ_{xy} of polycrystalline sample significantly exceeds that of the epitaxial one. This variation is mainly attributed to the difference in ρ_{xx} as previously mentioned. Furthermore, σ_{xy} of the polycrystalline Mn_3Ge was significantly reduced below 150 K, in contrast to the monotonic change in the epitaxial sample. The possible mechanisms underlying these trends are discussed below. The obtained σ_{xy} of both samples at 300 K are comparable to those of sputter-deposited Mn_3Sn films;[17,18,20,22,42] however, they were one order of magnitude smaller than those of bulk Mn_3Ge.[9,13] In addition, σ_{xy} of the polycrystalline Mn_3Ge film is slightly larger than that of the epitaxial one above 200 K. Such differences can be attributed to the extrinsic mechanisms of AHEs, which are originating from impurities and/or intermixing from adjacent layers.[22,43] The coercive field H_C is determined as H, and R_H is varied by half the value of the zero-field anomalous Hall resistance. Figure 4(f) summarizes the T dependence of H_C. The obtained $\mu_0 H_C$ of over 1.5 T in the epitaxial sample at 300 K is larger than that of epitaxial Mn_3Sn films.[22,42] The H_C of epitaxial Mn_3Ge decreases with T above 300 K, which is correlated with the temperature dependence of the magnetic anisotropy field displayed later. The H_C of the polycrystalline Mn_3Ge decreases with T above 300 K, which can be attributed to local pinning around the grain boundaries.

Furthermore, we investigated the magnetic anisotropy of a $(1\bar{1}00)$ oriented Mn_3Ge epitaxial film. The well-defined crystallographic configuration allows evaluation of magnetic anisotropy fields in the Kagome plane of non-collinear antiferromagnets.[29,31] In addition, we measured R_H while rotating the magnetic field in the Kagome plane of Mn_3Ge [Fig. 5(a)]. We define θ_H as the angle between the normal direction of the film and the magnetic field. A DC current was applied along the $[11\bar{2}0]$ direction of Mn_3Ge. With this setup, the change in the planar Hall resistance is negligible, and therefore, R_H vs magnetic field can be described as[29]

$$R_H \sim \frac{r_0}{t_{Mn3Ge}} \mu_0 H \cos\theta_H + R_{AHE} \cos\theta_M, \quad (1)$$

where r_0, R_{AHE}, t_{Mn_3Ge}, and θ_M represent the ordinary Hall coefficient, anomalous Hall resistance, Mn_3Ge thickness, and angle of magnetic order parameter from the film normal, respectively. Based on the rigid-body model, the magneto-static energy density u of Mn_3Ge is given by the sum of the densities of the Zeeman- and in-Kagome-plane magnetic anisotropic energies as[29,44]

$$u = -M_{UC} H \cos(\theta_M - \theta_H) + K_2 \sin^2\theta_M + \frac{K_4}{2}\cos 4\theta_M + \frac{K_6}{2}\cos 6\theta_M, \quad (2)$$

15 July 2024 07:27:53

© Author(s) 2024

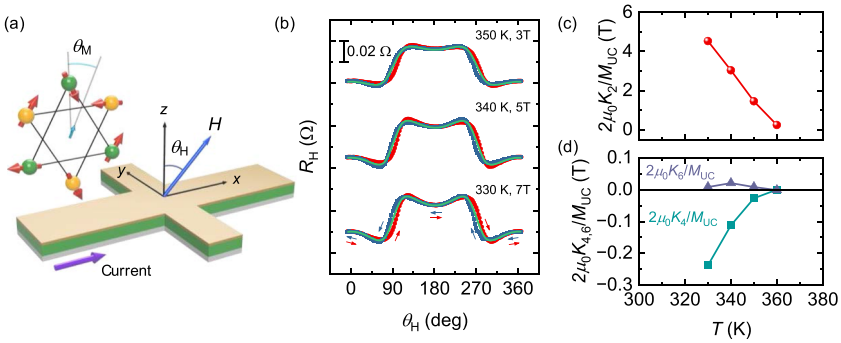

FIG. 5. (a) Schematic of a measurement system for the evaluation of magnetic anisotropies in the M-plane-oriented Mn_3Ge epitaxial film. (b) R_H vs θ_H for various temperatures and magnetic fields. The red (blue) plots are measured results for the process in which θ_H is changed from 0° (360)° to 360° (0)°. The green lines are the best-fit curves obtained by using Eqs. (1) and (2). Also shown is the T dependence of the effective magnetic anisotropy fields of (c) $2K_2/M_{UC}$ and (d) $2K_{4(6)}/M_{UC}$.

where M_{UC}, K_2, K_4, and K_6 represent the uncompensated magnetization and two-, four-, and sixfold magnetic anisotropy energy densities, respectively. Furthermore, K_2 and K_4 are induced by tensile strain, while K_6 originates from the symmetry of the crystal structure.[29,31] The magnetic field dependence of θ_M can be calculated numerically by the local-minimum condition of u given by $\frac{\partial u}{\partial \theta_M} = 0$ and $\frac{\partial^2 u}{\partial \theta_M^2} > 0$. Figure 5(b) illustrates R_H vs θ_H for various temperatures and magnetic fields. In addition, we observed a small hysteresis response in the measurement results, which can be attributed to the multi-domain formation of the Mn_3Ge film under the magnetic field sweep. A similar result has been reported in previous studies on Mn_3Sn films.[31] We evaluated the magnetic anisotropy fields $2K_2/M_{UC}$, $2K_4/M_{UC}$, and $2K_6/M_{UC}$ by fitting Eqs. (1) and (2) to the data at T = 330–360 K, where the hysteresis response was relatively small. Displayed in Figs. 5(c) and 5(d) is the T dependence of the evaluated $2K_2/M_{UC}$, $2K_4/M_{UC}$, and $2K_6/M_{UC}$. We found that $2K_2/M_{UC}$ was more than one order of magnitude larger than $2K_4/M_{UC}$ and $2K_6/M_{UC}$ and was the dominant contribution of K_2 to the in-Kagome-plane magnetic anisotropy. Furthermore, $2\mu_0K_2/M_{UC}$ obtained at 330 K is ~4 T, which is more than twice that

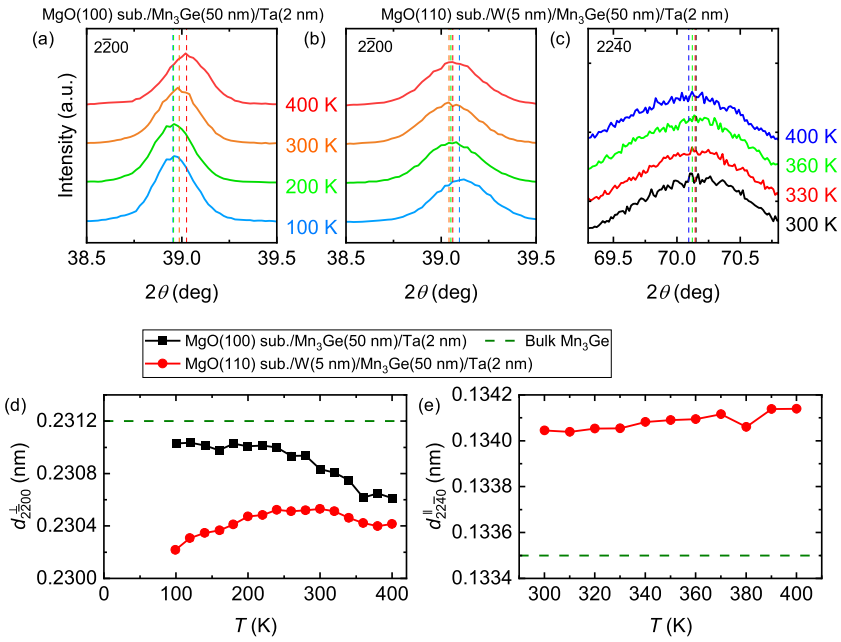

FIG. 6. Temperature-dependent out-of-plane XRD patterns in stacks with (a) polycrystalline and (b) epitaxial Mn_3Ge films. (c) In-plane XRD patterns of the epitaxial sample at different T. T dependence of the lattice spacing (d) $d^{\perp}_{2\bar{2}00}$ and (e) $d^{\parallel}_{22\bar{4}0}$. The dashed green lines denote the lattice spacing of bulk Mn_3Ge at room temperature.[45]

15 July 2024 07:27:53

© Author(s) 2024

of Mn_3Sn[29] at room temperature, thereby leading to high thermal stability in nanoscale devices.

We evaluated lattice constants at different T to further investigate the obtained T dependence of magnetic anisotropies and σ_{xy} in Mn_3Ge films. Figures 6(a) and 6(b) illustrate the out-of-plane XRD patterns of the polycrystalline and $(1\bar{1}00)$ oriented epitaxial Mn_3Ge films, respectively, at various temperatures. The views of the obtained XRD patterns are magnified near the positions of peaks from $Mn_3Ge(2\bar{2}00)$. We also evaluated another in-Kagome-plane lattice parameter of the epitaxial Mn_3Ge film by an in-plane XRD measurement (Fig. S2 of the supplementary material). In Fig. 6(c), the in-plane XRD patterns near the peaks from the $(22\bar{4}0)$ plane are displayed in the T range of 300–400 K. Figures 6(d) and 6(e) illustrate T dependence of the out-of-plane lattice spacing $d^{\perp}_{2\bar{2}00}$ and in-plane counterpart $d^{\parallel}_{22\bar{4}0}$, respectively. Here, $d^{\perp}_{2\bar{2}00}$ and $d^{\parallel}_{22\bar{4}0}$ of bulk Mn_3Ge at room temperature are also plotted.[45] The obtained $d^{\perp}_{2\bar{2}00}$ from the epitaxial film increased (decreased) with increasing T below (above) 300 K, whereas $d^{\parallel}_{22\bar{4}0}$ showed a monotonic increase with T above 300 K. These trends can be explained by the expansion of $d^{\parallel}_{22\bar{4}0}$ followed by the Poisson effect, leading to the reduction of $d^{\perp}_{2\bar{2}00}$, thereby suggesting that it contributed to the large $2K_2/M_{UC}$. A similar mechanism can also contribute to the monotonic increase in $d^{\perp}_{2\bar{2}00}$ vs T above 300 K for polycrystalline Mn_3Ge. Meanwhile, despite the enhancement of in-plane tensile strain with T above 300 K, $2K_2/M_{UC}$, and $2K_4/M_{UC}$ decreased by increasing T. In contrast, $2K_6/M_{UC}$ shows no significant change with respect to T. This can be attributed to the difference in whether the magnetic anisotropy is induced by the tensile strain or by the symmetry of the crystal structure. In polycrystalline Mn_3Ge, as shown in Fig. 6(d), although the strain is expected to be weaker than in epitaxial Mn_3Ge, the magnetic anisotropies can be also induced through a similar process.

Finally, we comment on the relationship between σ_{xy} and lattice parameters of Mn_3Ge films. Figure 4(e) illustrates that the obtained σ_{xy} vs T decreases monotonically for epitaxial Mn_3Ge, which is similar to that of bulk Mn_3Ge.[9,13] Meanwhile, the σ_{xy} of polycrystalline Mn_3Ge increases with T below 150 K. We obtained no strong correlation between the Hall conductivity and lattice parameters in the Mn_3Ge films, which sharply contrasts with the results for Mn_3Sn films.[42] A more detailed study is required to understand the mechanism of σ_{xy}–T.

In summary, we developed the epitaxial growth of $(1\bar{1}00)$ oriented non-collinear antiferromagnetic Mn_3Ge films with a large AHE. The temperature dependence of the anomalous Hall conductivity exhibited different trends for the epitaxial and polycrystalline Mn_3Ge films. Furthermore, we obtained a large in-Kagome-plane uniaxial magnetic anisotropy of epitaxial Mn_3Ge, which originated from the in-plane tensile strain, suggesting that high thermal stability and high robustness against the external field can be obtained in nanoscale devices. Our results offer insight into the design of future functional, high-speed, and high-density spintronic devices using antiferromagnets.

See the supplementary material for the magnetization measurement and in-plane XRD pattern of the MgO(110) substrate/W(5 nm)/Mn_3Ge(50 nm)/Ta(2 nm) stack.

The authors thank S. Fukami, Y. Yamane, Y. Sato, S. Mitani, and D. Ogawa for fruitful discussions and technical support. This work was partly supported by JSPS KAKENHI (Grant Nos. 22K14558, 22KK0072, 24K00952, and 24H00039), Casio Science Promotion Foundation (Grant No. 44-4), and Iketani Science and Technology Foundation (Grant No. 0361247-A).

AUTHOR DECLARATIONS

Conflict of Interest

The authors have no conflicts to disclose.

Author Contributions

Yutaro Takeuchi: Conceptualization (lead); Methodology (lead); Resources (equal); Investigation (lead); Data curation (lead); Formal analysis (lead); Funding acquisition (equal); Project administration (equal); Visualization (lead); Writing - Original draft (lead); Writing – Review & editing (equal); **Hossein Sepehri-Amin**: Resources (equal); Investigation (equal); Data curation (equal); Funding acquisition (equal); Visualization (equal); Writing - Review & editing (equal); **Satoshi Sugimoto**: Methodology (equal); Resources (equal); Investigation (equal); Funding acquisition (equal); Writing - Review & editing (equal); **Takanobu Hiroto**: Resources (equal); Investigation (equal); Data curation (equal); Visualization (equal); Writing - Review & editing (equal); **Shinya Kasai**: Methodology (equal); Funding acquisition (equal); Resources (equal); Investigation (equal); Supervision (lead); Writing - Original draft (equal); Writing - Review & editing (equal).

DATA AVAILABILITY

The data supporting the findings of this study are available from the corresponding authors upon reasonable request.

REFERENCES

[1] S. Bhatti, R. Sbiaa, A. Hirohata, H. Ohno, S. Fukami, and S. N. Piramanayagam, Mater. Today **20**, 530 (2017).
[2] B. Dieny, I. L. Prejbeanu, K. Garello, P. Gambardella, P. Freitas, R. Lehndorff, W. Raberg, U. Ebels, S. O. Demokritov, J. Akerman, A. Deac, P. Pirro, C. Adelmann, A. Anane, A. V. Chumak, A. Hirohata, S. Mangin, S. O. Valenzuela, M. C. Onbaşlı, M. d'Aquino, G. Prenat, G. Finocchio, L. Lopez-Diaz, R. Chantrell, O. Chubykalo-Fesenko, and P. Bortolotti, Nat. Electron. **3**, 446 (2020).
[3] J. Grollier, D. Querlioz, K. Y. Camsari, K. Everschor-Sitte, S. Fukami, and M. D. Stiles, Nat. Electron. **3**, 360 (2020).
[4] P. Wadley, B. Howells, J. elezny, C. Andrews, V. Hills, R. P. Campion, V. Novak, K. Olejnik, F. Maccherozzi, S. S. Dhesi, S. Y. Martin, T. Wagner, J. Wunderlich, F. Freimuth, Y. Mokrousov, J. Kune, J. S. Chauhan, M. J. Grzybowski, A. W. Rushforth, K. W. Edmonds, B. L. Gallagher, and T. Jungwirth, Science **351**, 587 (2016).
[5] T. Jungwirth, X. Marti, P. Wadley, and J. Wunderlich, Nat. Nanotechnol. **11**, 231 (2016).
[6] V. Baltz, A. Manchon, M. Tsoi, T. Moriyama, T. Ono, and Y. Tserkovnyak, Rev. Mod. Phys. **90**, 015005 (2018).
[7] J. Železný, P. Wadley, K. Olejník, A. Hoffmann, and H. Ohno, Nat. Phys. **14**, 220 (2018).

15 July 2024 07:27:53

© Author(s) 2024

[8]S. Nakatsuji, N. Kiyohara, and T. Higo, Nature **527**, 212 (2015).
[9]A. K. Nayak, J. E. Fischer, Y. Sun, B. Yan, J. Karel, A. C. Komarek, C. Shekhar, N. Kumar, W. Schnelle, J. Kübler, C. Felser, and S. S. P. Parkin, Sci. Adv. **2**, e1501870 (2016).
[10]Z. Feng, X. Zhou, L. Šmejkal, L. Wu, Z. Zhu, H. Guo, R. González-Hernández, X. Wang, H. Yan, P. Qin, X. Zhang, H. Wu, H. Chen, Z. Meng, L. Liu, Z. Xia, J. Sinova, T. Jungwirth, and Z. Liu, Nat. Electron. **5**, 735 (2022).
[11]R. D. Gonzalez Betancourt, J. Zubáč, R. Gonzalez-Hernandez, K. Geishendorf, Z. Šobáň, G. Springholz, K. Olejník, L. Šmejkal, J. Sinova, T. Jungwirth, S. T. B. Goennenwein, A. Thomas, H. Reichlová, J. Železný, and D. Kriegner, Phys. Rev. Lett. **130**, 036702 (2023).
[12]T. Higo, H. Man, D. B. Gopman, L. Wu, T. Koretsune, O. M. J. van 't Erve, Y. P. Kabanov, D. Rees, Y. Li, M.-T. Suzuki, S. Patankar, M. Ikhlas, C. L. Chien, R. Arita, R. D. Shull, J. Orenstein, and S. Nakatsuji, Nat. Photonics **12**, 73 (2018).
[13]N. Kiyohara, T. Tomita, and S. Nakatsuji, Phys. Rev. Appl. **5**, 064009 (2016).
[14]K.-R. Jeon, B. K. Hazra, K. Cho, A. Chakraborty, J.-C. Jeon, H. Han, H. L. Meyerheim, T. Kontos, and S. S. P. Parkin, Nat. Mater. **20**, 1358 (2021).
[15]K.-R. Jeon, B. K. Hazra, J.-K. Kim, J.-C. Jeon, H. Han, H. L. Meyerheim, T. Kontos, A. Cottet, and S. S. P. Parkin, Nat. Nanotechnol. **18**, 747 (2023).
[16]Z. Q. Liu, H. Chen, J. M. Wang, J. H. Liu, K. Wang, Z. X. Feng, H. Yan, X. R. Wang, C. B. Jiang, J. M. D. Coey, and A. H. MacDonald, Nat. Electron. **1**, 172 (2018).
[17]T. Higo, D. Qu, Y. Li, C. L. Chien, Y. Otani, and S. Nakatsuji, Appl. Phys. Lett. **113**, 202402 (2018).
[18]T. Ikeda, M. Tsunoda, M. Oogane, S. Oh, T. Morita, and Y. Ando, Appl. Phys. Lett. **113**, 222405 (2018).
[19]H. Reichlova, T. Janda, J. Godinho, A. Markou, D. Kriegner, R. Schlitz, J. Zelezny, Z. Soban, M. Bejarano, H. Schultheiss, P. Nemec, T. Jungwirth, C. Felser, J. Wunderlich, and S. T. B. Goennenwein, Nat. Commun. **10**, 5459 (2019).
[20]Y. You, X. Chen, X. Zhou, Y. Gu, R. Zhang, F. Pan, and C. Song, Adv. Electron. Mater. **5**, 1800818 (2019).
[21]H. Bai, W. Zhu, Y. You, X. Chen, X. Zhou, F. Pan, and C. Song, Appl. Phys. Lett. **117**, 052404 (2020).
[22]J. Yoon, Y. Takeuchi, R. Itoh, S. Kanai, S. Fukami, and H. Ohno, Appl. Phys. Express **13**, 013001 (2020).
[23]H. Iwaki, M. Kimata, T. Ikebuchi, Y. Kobayashi, K. Oda, Y. Shiota, T. Ono, and T. Moriyama, Appl. Phys. Lett. **116**, 022408 (2020).
[24]M. Raju, R. Romero, D. Nishio-Hamane, R. Uesugi, M. Asakura, Z. Tagay, T. Higo, N. P. Armitage, C. Broholm, and S. Nakatsuji, Phys. Rev. Mater. **8**, 014204 (2024).
[25]H. Tsai, T. Higo, K. Kondou, T. Nomoto, A. Sakai, A. Kobayashi, T. Nakano, K. Yakushiji, R. Arita, S. Miwa, Y. Otani, and S. Nakatsuji, Nature **580**, 608 (2020).
[26]Y. Takeuchi, Y. Yamane, J.-Y. Yoon, R. Itoh, B. Jinnai, S. Kanai, J. Ieda, S. Fukami, and H. Ohno, Nat. Mater. **20**, 1364 (2021).
[27]H. Xie, X. Chen, Q. Zhang, Z. Mu, X. Zhang, B. Yan, and Y. Wu, Nat. Commun. **13**, 5744 (2022).
[28]B. Pal, B. K. Hazra, B. Göbel, J.-C. Jeon, A. K. Pandeya, A. Chakraborty, O. Busch, A. K. Srivastava, H. Deniz, J. M. Taylor, H. Meyerheim, I. Mertig, S.-H. Yang, and S. S. P. Parkin, Sci. Adv. **8**, eabo5930 (2022).
[29]T. Higo, K. Kondou, T. Nomoto, M. Shiga, S. Sakamoto, X. Chen, D. Nishio-Hamane, R. Arita, Y. Otani, S. Miwa, and S. Nakatsuji, Nature **607**, 474 (2022).
[30]G. Q. Yan, S. Li, H. Lu, M. Huang, Y. Xiao, L. Wernert, J. A. Brock, E. E. Fullerton, H. Chen, H. Wang, and C. R. Du, Adv. Mater. **34**, 2200327 (2022).
[31]J.-Y. Yoon, P. Zhang, C.-T. Chou, Y. Takeuchi, T. Uchimura, J. T. Hou, J. Han, S. Kanai, H. Ohno, S. Fukami, and L. Liu, Nat. Mater. **22**, 1106 (2023).
[32]X. Chen, T. Higo, K. Tanaka, T. Nomoto, H. Tsai, H. Idzuchi, M. Shiga, S. Sakamoto, R. Ando, H. Kosaki, T. Matsuo, D. Nishio-Hamane, R. Arita, S. Miwa, and S. Nakatsuji, Nature **613**, 490 (2023).
[33]P. Qin, H. Yan, X. Wang, H. Chen, Z. Meng, J. Dong, M. Zhu, J. Cai, Z. Feng, X. Zhou, L. Liu, T. Zhang, Z. Zeng, J. Zhang, C. Jiang, and Z. Liu, Nature **613**, 485 (2023).
[34]T. Ogasawara, J. Kim, Y. Ando, and A. Hirohata, J. Magn. Magn. Mater. **473**, 7 (2019).
[35]P. Qin, Z. Feng, X. Zhou, H. Guo, J. Wang, H. Yan, X. Wang, H. Chen, X. Zhang, H. Wu, Z. Zhu, and Z. Liu, ACS Nano **14**, 6242 (2020).
[36]X. Wang, C. Zhang, Q. Yang, L. Liu, D. Pan, X. Chen, J. Deng, T. Zhai, and H.-X. Deng, APL Mater. **9**, 111107 (2021).
[37]D. Hong, N. Anand, C. Liu, H. Liu, I. Arslan, J. E. Pearson, A. Bhattacharya, and J. S. Jiang, Phys. Rev. Mater. **4**, 094201 (2020).
[38]D. Hong, C. Liu, J. Wen, Q. Du, B. Fisher, J. S. Jiang, J. E. Pearson, and A. Bhattacharya, APL Mater. **10**, 101113 (2022).
[39]T. Nagamiya, S. Tomiyoshi, and Y. Yamaguchi, Solid State Commun. **42**, 385 (1982).
[40]S. Tomiyoshi, Y. Yamaguchi, and T. Nagamiya, J. Magn. Magn. Mater. **31–34**, 629 (1983).
[41]J. Liu and L. Balents, Phys. Rev. Lett. **119**, 087202 (2017).
[42]J.-Y. Yoon, Y. Takeuchi, S. DuttaGupta, Y. Yamane, S. Kanai, J. Ieda, H. Ohno, and S. Fukami, AIP Adv. **11**, 065318 (2021).
[43]A. Markou, D. Kriegner, J. Gayles, L. Zhang, Y.-C. Chen, B. Ernst, Y.-H. Lai, W. Schnelle, Y.-H. Chu, Y. Sun, and C. Felser, Phys. Rev. B **100**, 054422 (2019).
[44]Y. Sato, Y. Takeuchi, Y. Yamane, J.-Y. Yoon, S. Kanai, J. Ieda, H. Ohno, and S. Fukami, Appl. Phys. Lett. **122**, 122404 (2023).
[45]H. Niida, T. Hori, Y. Yamaguchi, and Y. Nakagawa, J. Appl. Phys. **73**, 5692 (1993).

15 July 2024 07:27:53

© Author(s) 2024